galaxies

MDPI

Article

Steps toward Unraveling the Structure and Formation of Five Polar Ring Galaxies

Kyle E. Lackey [1,*], Varsha P. Kulkarni [1,*], Monique C. Aller [2,*]

[1] Department of Physics and Astronomy, University of South Carolina, Columbia, SC 29208, USA
[2] Department of Biochemistry, Chemistry and Physics, Georgia Southern University, Statesboro, GA 30458, USA
* Correspondence: lackeyk@email.sc.edu (K.E.L.); kulkarni@sc.edu (V.P.K.); maller@georgiasouthern.edu (M.C.A.)

Abstract: Polar ring galaxies (PRGs) are unusual relative to common galaxies in that they consist of a central host galaxy—usually a gas-poor, early-type S0 or elliptical galaxy—surrounded by a ring of gas, dust and stars that orbit perpendicular to the major axis of the host. Despite the general quiescence of early-type galaxies (ETGs) and the rings' lack of spiral density waves, PRGs are the sites of significant star formation relative to typical ETGs. To study these structures and improve PRG statistics, we obtained and analyzed infrared (IR) images from the Infrared Array Camera (IRAC) aboard the Spitzer Space Telescope, and combined these IR data with archival optical data from both the Sloan Digital Sky Survey and the Hubble Space Telescope, and with optical imaging data we obtained with the Gemini South Observatory. We performed structural decomposition and photometry for five PRGs, and fit the spectral energy distributions (SEDs) of each PRG component to estimate the stellar masses, ages, and other physical properties of the PRG components. We show that PRC B-12 and PRC B-22, both lacking previous analysis, obey trends commonly observed among PRGs. We find that the stellar masses of polar rings can be a significant fraction of the host galaxy's stellar masses (∼10–30%). We note, however, that our estimates of stellar mass and other physical properties are the results of SED fitting and not direct measurements. Our findings corroborate both previous theoretical expectations and measurements of existing samples of PRGs and indicate the utility of SED fitting in the context of these unusual galaxies, which historically have lacked multi-wavelength photometry of their stellar components. Finally, we outline future improvements needed for more definitive studies of PRGs and their formation scenarios.

Keywords: polar ring galaxies; irregular galaxies; galaxy formation

Citation: Lackey, K.E.; Kulkarni, V.P.; Aller, M.C. Steps toward Unraveling the Structure and Formation of Five Polar Ring Galaxies. *Galaxies* **2024**, *12*, 42. https://doi.org/10.3390/galaxies12040042

Academic Editor: Oleg Malkov

Received: 5 April 2024
Revised: 17 July 2024
Accepted: 30 July 2024
Published: 31 July 2024

1. Introduction

Polar ring galaxies (PRGs) are unusual systems composed of a central host, typically an early-type galaxy (ETG) surrounded by a ring of gas, dust, and stars orbiting at an orientation nearly perpendicular to that of the host [1]. We note, however, that polar rings have been discovered around non-ETGs such as NGC 660, and possibly also detected in gas around NGC 4632 and NGC 6156 (e.g., [2]). The polar ring itself exhibits a large amount of neutral hydrogen gas, a trait often associated with late-type galaxies [3]. PRGs are not common in the local universe, only about 0.5% of nearby S0 galaxies host a polar ring [1,4], and only a handful of catalogs exist to document the population (e.g., [1,5,6], though the number seems likely to increase.

There are a few theories that attempt to explain PRG formation: (a) accretion, wherein two galaxies interact in such a way that one strip mass from the other [7]; (b) galaxy mergers, where two galaxies collide and shred each other [8,9]; (c) cosmic formation when PRGs coalesce along cosmic filaments [10,11]. In particular, simulations of the accretion model suggest that the mass of the polar ring is related to the central mass concentration of the

host galaxy: elliptical hosts form smaller rings, while S0 hosts with extended, massive dark matter halos form larger rings. The S0 galaxies themselves may result from a polar merger of two disk galaxies with unequal masses [12].

In terms of the formation of stars, PRGs present an environment distinct from the disks of spirals for a number of reasons. The polar rings show extended star formation throughout their structures even though there is no density wave in the ring to trigger star formation. Moreover, the density of the ring ISM is likely to be low, since the ring is far from the center of the galaxy's potential well. Despite these factors, young star populations are visible within the rings.

An additional problem, besides the low numbers of PRGs, is that studies often present results taken from the host-ring system as a whole, rather than differentiating between components (e.g., the polar ring, the host's galactic bulge, and the host's galactic disk, where the latter exists). This results in both photometry and physical parameterization that blend the traits of visually distinct structures, which ultimately hinders any attempts to trace the history of a given PRG. The main thrust of this paper is to study the photometry of distinct components of PRGs, and to estimate each component's age, mass, and star formation rate (SFR), thereby facilitating a more efficient assessment of trends within the growing population of polar rings. Furthermore, such decomposition of the host-ring systems may afford insight into whether any of the above formation scenarios are more frequent than the others.

In this work, we adopt a standard, flat ΛCDM cosmology with $\Omega_m = 0.3$, $\Omega_\Lambda = 0.7$, and $H_0 = 70$ km s^{-1} Mpc^{-1}.

2. Materials and Methods

2.1. Observations

Our sample includes five well-defined PRGs from the catalog of [1]; see Table 1. Each target boasts a ring that is approximately edge-on to our line of sight so that modeling the polar structures is simpler.

Table 1. Our Sample of Polar Ring Galaxies. Redshifts, galactic extinctions, and coordinates taken from the NASA/IPAC Extragalactic Database.

Galaxy ID	z	A_V	R.A.	Dec.
PRC A-4 (UGC 7576)	0.023406	0.061	12:27:41.8594	+28:41:53.077
PRC A-5 (NGC 4650A)	0.009607	0.312	12:44:49.0600	−40:42:51.500
PRC A-6 (UGC 9796)	0.017980	0.073	15:15:56.3481	+43:09:59.889
PRC B-12 (ESO 503- G 017)	0.034907	0.171	11:26:52.5500	−27:42:20.900
PRC B-22 (AM 2329-410)	0.045312	0.051	23:31:54.6100	−40:45:43.600

For each PRG, we use data from multiple instruments across many wavebands; see Table 2. Observations of each PRG were obtained with the Infrared Array Camera (IRAC) aboard NASA's Spitzer Space Telescope (SST) in two bands, "Channel 1" and "Channel 2", centered at wavelengths of 3.6 μm and 4.5 μm, respectively, as part of Spitzer GO programs 70165 and 80194 (PI Kulkarni). We have also used the Gemini-South Observatory Multi-Object Spectrograph (GMOS-S) in its imaging mode to collect optical data in three bands, "g", "r", and "i", centered at wavelengths of 475 nm, 630 nm, and 780 nm, respectively, as part of Gemini-S program Gs-2012A-O-56 (PI Aller). To our knowledge, neither PRC B-12 nor PRC B-22 had sufficient resolution and multiwavelength optical data prior to this undertaking. Additional archival data from the Hubble Space Telescope, Wide Field

Planetary Camera 2 (HST-WFPC2; program ID 8399, PI Noll) and the Sloan Digital Sky Survey (SDSS) were also used. PRC A-4, A-5, B-12, and B-22 also have mid-infrared (MIR) imaging from the Wide-Field Infrared Survey Explorer (WISE). New observations may yield improved results for objects with older data.

We stress that multi-wavelength data are essential for our purposes. While optical data are sufficient for the study of the stellar component, IR data are essential to correct for dust extinction effects and to obtain accurate stellar masses. Furthermore, the IR data better trace the older and lower mass stellar population than the optical data.

Table 2. Details of Observations for sample of PRGs.

Galaxy ID	Instrument, Filter	Number of Exposures	Total Exposure Time (s)	PSF FWHM (pc)
PRC A-4	SDSS, g	1	53.9	254.9
	SDSS, r	1	53.9	292.6
	SDSS, i	1	53.9	302.1
	IRAC, 3.6 μm	200	4720	783.5
	IRAC, 4.5 μm	200	5360	811.8
PRC A-5	WFPC2, F450W	8	7700	19.7
	WFPC2, F606W	6	4803	29.6
	WFPC2, F814W	8	7660	39.4
	IRAC, 3.6 μm	40	944	327.0
	IRAC, 4.5 μm	40	1072	338.8
PRC A-6	SDSS, g	1	53.9	197.1
	SDSS, r	1	53.9	226.3
	SDSS, i	1	53.9	233.6
	IRAC, 3.6 μm	200	4720	605.9
	IRAC, 4.5 μm	200	5360	627.8
PRC B-12	GMOS-S, g	7	2100	375.3
	GMOS-S, r	4	1200	430.9
	GMOS-S, i	6	1800	444.8
	IRAC, 3.6 μm	280	6608	1153.7
	IRAC, 4.5 μm	280	7504	1195.4
PRC B-22	GMOS-S, g	5	1500	481.1
	GMOS-S, r	4	1200	552.4
	GMOS-S, i	6	1800	570.2
	IRAC, 3.6 μm	200	4720	1479.1
	IRAC, 4.5 μm	200	5360	1532.5

2.2. Data Reduction

The IR images were processed using the Spitzer IRAC pipeline and mosaic images were produced using the MOsaicker and Point source EXtractor (MOPEX) software package provided by the Spitzer Science Center [13]. The optical Gemini images were processed using the Data Reduction for Astronomy from Gemini Observatory North and South (DRAGONS) software package provided by the Gemini North-South Observatory [14]. The SDSS and HST images were downloaded from the SDSS DR12 and Hubble Legacy Archives, respectively, and were not further processed.

We used the Overlap and Mosaic pipelines in MOPEX for the IRAC 3.6 μm and 4.5 μm data. In the Mosaic pipeline, we chose a Mosaic Interpolate method of "Drizzle" with "Drizzle Factor = 0.65", we removed the Mosaic Reinterpolate module, which disables outlier rejection while interpolating with Drizzle, and we added the Mosaic Med Filter module. For galaxies with high coverage (e.g., 10 or more frames), there is no appreciable difference in the resultant data products between the Drizzle and Default interpolation methods. Adding the Mosaic Med Filter module into the processing flow serves to retain a version of the final mosaic with the sky background subtracted, which is helpful in

conducting the photometry. The resulting mosaics of the PRGs were in units of MJy/sr, which were converted into units of counts for performing photometry.

We employed DRAGONS according to the "GMOS Imaging Data Reduction Tutorial" available online. The resulting mosaics of the PRGs were in units of electrons, which is appropriate for performing photometry.

2.3. Photometry

The 2-D decomposition of the galaxies was performed using the software package GALFIT [15,16] that can decompose a galaxy into its different components (e.g., a disk, a central bulge, and a polar ring), and report the basic shape (e.g., position angle and ellipticity) and parameters of the light distribution (e.g., integrated magnitude and effective radius) for each component, based on the user's initial setup. In our case, all five of the host galaxies are classified as lenticular (S0), so we adopt a three-component model for each PRG, allowing for a polar structure, a host galactic disk, and a host galactic bulge.

Since the uncertainties produced by the data reduction were negligible, and to introduce as few opportunities for error as possible, we had GALFIT produce a sigma image for each mosaic, which requires that the data be in units of either counts or electrons. We, therefore, converted the Spitzer, HST, and SDSS images; appropriate conversion factors typically reside within the image headers of the data.

For a PSF, in each PRG mosaic, we chose an isolated star without saturation, cropped it into its own image that was centered on the star, and normalized that image. We then provided this to GALFIT as the convolution kernel for its modeling.

In order to generate the mask files for use in GALFIT, we first constructed segmentation maps using SExtractor [17] on each mosaic image, and assigned all objects other than those associated with the PRG to be masked, so that GALFIT modeled only the PRG and sky background.

For the fitting, we adopted a single Sérsic function with seven free parameters (x-y coordinates, integrated magnitude, effective radius, Sérsic index, ellipticity, and position angle) for each of the three components. Since each ring is approximately edge-on, we forego any truncation. We also include a sky function to account for any residual background light, so that it is not assigned to the PRG.

The formal uncertainties for the various parameters returned by GALFIT were found to be unrealistically low. In order to estimate more reasonable uncertainties on the photometric magnitudes (which are the only photometric parameter needed for our goal of SED fitting), we ran GALFIT 1000 times on each galaxy, keeping the integrated magnitude a free parameter, but restricting the other six parameters to random values within a $\pm 2\sigma$ range of their initial solutions. The standard deviation of the 1000 magnitudes thus computed was then adopted as the magnitude uncertainty, for each band for each PRG, to provide meaningful measurement uncertainties for later SED-fitting.

2.4. SED Fitting

In order to estimate the ages, masses, and SFRs of the rings and host galaxies we used the galaxy SED-fitting program, CIGALE (Code Investigating GALaxy Emission; [18]).

To model the star formation history, we used the "sfhdelayed" module (delayed SFH with exponential burst), characterized by five parameters: the e-folding times of the star formation timescales for the main stellar population (*tau_main* = 500, 1000, 3000, 5000 Myr) and the late starburst population (*tau_burst* = 100, 500, 1000, 3000 Myr), the ages of the main stellar population (*age_main* = 2500, 3000, 5000, 8000, 10,000 Myr) and the late starburst (*age_burst* = 500, 1000, 1500, 2000 Myr), and the mass fraction of the late starburst population (*f_burst* = 0.0, 0.1, 0.2, 0.3, 0.4, 0.5).

We used the Bruzual and Charlot stellar population synthesis models ([19]) with the Chabrier initial mass function, all permitted metallicity values (*metallicity* = 0.0001, 0.0004, 0.004, 0.008, 0.02, 0.05), and fixed the age of separation delineating the young and old star populations to 10 Myr (*separation_age*).

To model the dust attenuation, we used the Calzetti attenuation law ([20]; specifically *dustatt_calzleit* in CIGALE), varying the color excess of the stellar continuum light for the young star population in steps of 0.1, from 0.0 to 2.0. To model the dust emission, we used dust emission templates from [21]. To model nebular emission, we used the lone "nebular" module, opting to have CIGALE use every possible value of both *gas metallicity* (26 values between 0.000 and 0.051) and *electron density* (10 cm^{-3}, 100 cm^{-3}, 1000 cm^{-3}).

In summary, a total of $\sim 10^7$ to $\sim 10^8$ models were run for each PRG. From this CIGALE chooses a "best-fit" model via χ^2 minimization—from which an SED is plotted—but also performs a Bayesian-like analysis, by way of which the physical properties are not determined according to the best-fit model, but by weighting all of the combinations by the likelihood of each, with the best-fit models having the greatest weight [18]. What separates CIGALE's analysis from true Bayesian statistics is the program's lack of a formal prior, otherwise, it applies similar conventions. It is this "Bayesian-like" method that provides the uncertainties in our results, and thus we consider the "Bayesian" parameters to be more reliable options over the best-fit parameters.

3. Results

3.1. Photometry

Figure 1 displays the five target galaxies, in addition to their GALFIT models and residuals, the ring and host galaxy are readily apparent in the data. The residuals—in this case, the model subtracted from the data—show structures within the rings and disks, and occasionally a central light source which might be attributed to an AGN or nuclear star cluster at the center of the PRG.

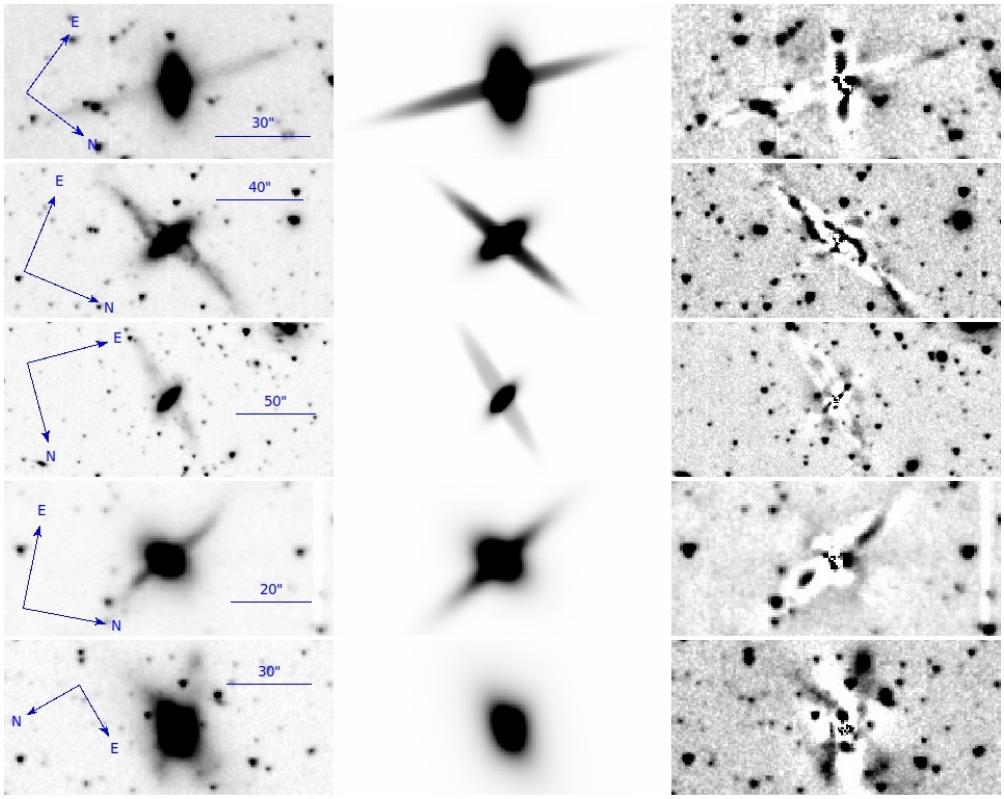

Figure 1. From left to right: IRAC 3.6 μm images, GALFIT models, and difference residuals (*data* − *model*) for the target galaxy sample. IRAC 4.5 μm images, models, and residuals are visually similar and so are not plotted. From top to bottom: PRC A-4, PRC A-5, PRC A-6, PRC B-12, and PRC B-22.

Tables 3–7 detail the properties of the light profiles for each of the three components in each of the five targets according to GALFIT, at each of the five wavebands per target.

While each parameter is given with its uncertainty, those of the AB magnitudes are more robust (derived as mentioned above). The uncertainties for the other parameters are the formal values returned by GALFIT and may be underestimated.

Table 3. GALFIT results for PRC A-4. Columns, left to right: the component in question, the instrument filter, the integrated AB Magnitude, the effective radius of the light profile, the Sérsic index, the ellipticity, and the position angle of the component measured East of North in degrees. Where a quantity has no uncertainty, GALFIT reported a formal uncertainty of 0.00.

Component	Filter	Magnitude (AB)	r_e (kpc)	n	e	P.A.
PRC A-4	g	16.78 ± 0.06	14.56 ± 0.01	0.36 ± 0.01	0.10	52.96 ± 0.08
polar ring	r	16.30 ± 0.07	15.18 ± 0.12	0.40 ± 0.01	0.10	52.96 ± 0.08
	i	15.87 ± 0.08	15.85 ± 0.16	0.43 ± 0.02	0.10	52.99 ± 0.07
	3.6 µm	14.99 ± 0.03	12.57 ± 0.14	0.28 ± 0.01	0.10	52.28 ± 0.07
	4.5 µm	15.51 ± 0.02	12.95 ± 0.16	0.24 ± 0.01	0.10	52.46 ± 0.08
PRC A-4	g	17.56 ± 0.02	0.49 ± 0.002	0.49 ± 0.01	0.91	18.57 ± 3.50
host bulge	r	16.77 ± 0.02	0.49 ± 0.002	0.66	0.88	23.95 ± 1.79
	i	16.19 ± 0.02	0.49 ± 0.002	0.65	0.93	35.91 ± 2.27
	3.6 µm	13.97 ± 0.02	0.68 ± 0.006	0.54 ± 0.01	0.82	25.64 ± 1.72
	4.5 µm	14.61 ± 0.03	0.69 ± 0.009	0.55 ± 0.01	0.83	26.72 ± 2.43
PRC A-4	g	15.82 ± 0.01	3.16 ± 0.02	1.45 ± 0.01	0.48	133.78 ± 0.14
host disk	r	15.01 ± 0.01	3.12 ± 0.02	1.63 ± 0.02	0.45	132.98 ± 0.10
	i	14.56 ± 0.01	3.13 ± 0.02	1.63 ± 0.02	0.45	133.01 ± 0.10
	3.6 µm	12.75 ± 0.01	2.32 ± 0.02	1.33 ± 0.01	0.51	131.67 ± 0.16
	4.5 µm	13.36 ± 0.01	2.33 ± 0.02	1.34 ± 0.01	0.51	131.14 ± 0.19

Table 4. GALFIT results for PRC A-5. Format identical to Table 3.

Component	Filter	Magnitude (AB)	r_e (kpc)	n	e	P.A.
PRC A-5	F450W	15.05 ± 0.06	6.92 ± 0.01	0.47	0.14	161.60 ± 0.01
polar ring	F606W	14.69 ± 0.06	6.48 ± 0.01	0.48	0.15	161.98 ± 0.01
	F814W	14.48 ± 0.06	6.12 ± 0.01	0.50	0.15	162.33 ± 0.02
	3.6 µm	12.85 ± 0.04	5.12 ± 0.01	0.30	0.13	162.06 ± 0.03
	4.5 µm	13.47 ± 0.04	5.12 ± 0.02	0.28	0.13	162.48 ± 0.04
PRC A-5	F450W	16.69 ± 0.01	0.15 ± 0.0004	2.26	0.91	91.41 ± 0.37
host bulge	F606W	16.09 ± 0.01	0.19 ± 0.0002	1.33	0.87	81.67 ± 0.20
	F814W	15.47 ± 0.01	0.20 ± 0.0002	1.60	0.89	84.87 ± 0.21
	3.6 µm	13.55 ± 0.02	0.29 ± 0.002	0.81 ± 0.01	0.91 ± 0.01	70.84 ± 2.64
	4.5 µm	14.13 ± 0.03	0.31 ± 0.004	0.92 ± 0.01	0.90 ± 0.01	69.97 ± 2.79
PRC A-5	F450W	15.10 ± 0.02	2.10 ± 0.003	1.12	0.37	61.70 ± 0.03
host disk	F606W	14.35 ± 0.02	2.03 ± 0.002	1.03	0.37	61.90 ± 0.02
	F814W	13.79 ± 0.02	1.96 ± 0.002	1.03	0.37	61.87 ± 0.01
	3.6 µm	11.90 ± 0.01	1.59 ± 0.005	0.85	0.41	60.53 ± 0.06
	4.5 µm	12.55 ± 0.01	1.62 ± 0.007	0.86 ± 0.01	0.41	60.92 ± 0.07

Table 5. GALFIT results for PRC A-6. Format identical to Table 3.

Component	Filter	Magnitude (AB)	r_e (kpc)	n	e	P.A.
PRC A-6	g	16.36 ± 0.04	12.11 ± 0.10	0.29 ± 0.01	0.19	14.74 ± 0.10
polar ring	r	15.84 ± 0.04	10.76 ± 0.10	0.37 ± 0.01	0.22	14.83 ± 0.15
	i	15.43 ± 0.04	10.36 ± 0.13	0.46 ± 0.01	0.23	14.84 ± 0.20
	3.6 µm	14.31 ± 0.03	10.51 ± 0.03	0.22	0.15	16.20 ± 0.05
	4.5 µm	15.06 ± 0.04	10.93 ± 0.06	0.18 ± 0.01	0.13	16.29 ± 0.08
PRC A-6	g	17.76 ± 0.01	0.35 ± 0.001	0.67 ± 0.01	0.90	165.87 ± 3.24
host bulge	r	16.91 ± 0.01	0.34 ± 0.001	0.71	0.96	115.80 ± 4.68
	i	16.45 ± 0.01	0.35 ± 0.001	0.75	0.96 ± 0.01	115.27 ± 4.52
	3.6 µm	14.23 ± 0.02	0.47 ± 0.002	0.65 ± 0.01	0.83	100.25 ± 1.80
	4.5 µm	15.00 ± 0.05	0.48 ± 0.01	0.66 ± 0.02	0.86 ± 0.01	109.36 ± 3.98
PRC A-6	g	16.24 ± 0.02	2.33 ± 0.02	1.15 ± 1.15	0.38	124.38 ± 0.14
host disk	r	15.45 ± 0.01	2.25 ± 0.01	1.11 ± 0.01	0.38	124.01 ± 0.10
	i	15.03 ± 0.02	2.25 ± 0.01	1.09 ± 0.01	0.37	123.91 ± 0.10
	3.6 µm	12.95 ± 0.01	1.37 ± 0.01	0.94 ± 0.01	0.43	125.50 ± 0.09
	4.5 µm	13.58 ± 0.01	1.41 ± 0.02	0.95 ± 0.01	0.43	126.28 ± 0.18

Table 6. GALFIT results for PRC B-12. Format identical to Table 3. The asterisk indicates that the Sersic Index parameter was held fixed at the constant value in GALFIT operations.

Component	Filter	Magnitude (AB)	r_e (kpc)	n	e	P.A.
PRC B-12 polar ring	g	17.64 ± 0.05	10.04 ± 0.03	1.68	0.19	53.17 ± 0.02
	r	16.82 ± 0.06	9.95 ± 0.00 *	2.13	0.19	52.65 ± 0.03
	i	16.33 ± 0.14	9.99 ± 0.02	1.29	0.17	51.19 ± 0.02
	3.6 µm	14.40 ± 0.04	8.80 ± 0.08	0.73 ± 0.01	0.19	52.64 ± 0.09
	4.5 µm	15.02 ± 0.04	8.39 ± 0.07	0.65 ± 0.01	0.19	52.48 ± 0.09
PRC B-12 host bulge	g	18.93 ± 0.01	0.52 ± 0.001	0.57	0.75	52.32 ± 0.15
	r	17.70 ± 0.01	0.44 ± 0.001	0.66	0.78	55.74 ± 0.11
	i	17.14 ± 0.02	0.38 ± 0.001	0.88	0.83	46.17 ± 0.17
	3.6 µm	14.33 ± 0.10	0.95 ± 0.004	0.47 ± 0.01	0.82 ± 0.01	26.84 ± 2.07
	4.5 µm	14.98 ± 0.05	0.81 ± 0.008	0.50	0.93 ± 0.01	20.92 ± 5.69
PRC B-12 host disk	g	16.87 ± 0.02	3.69 ± 0.005	1.56	0.54	151.69 ± 0.04
	r	15.90 ± 0.02	3.19 ± 0.003	1.55	0.55	153.02 ± 0.03
	i	15.43 ± 0.02	2.91 ± 0.002	1.71	0.56	153.02 ± 0.02
	3.6 µm	13.05 ± 0.03	2.53 ± 0.02	1.60 ± 0.01	0.66	150.16 ± 0.27
	4.5 µm	13.79 ± 0.02	2.61 ± 0.02	1.16 ± 0.01	0.67	150.87 ± 0.32

Table 7. GALFIT results for PRC B-22. Format identical to Table 3.

Component	Filter	Magnitude (AB)	r_e (kpc)	n	e	P.A.
PRC B-22 polar ring	g	16.36 ± 0.01	7.00 ± 0.01	1.39	0.59	36.84 ± 0.05
	r	16.07 ± 0.04	9.76 ± 0.01	0.77	0.47	36.33 ± 0.02
	i	16.06 ± 0.04	7.18 ± 0.01	0.42	0.53	32.75 ± 0.03
	3.6 µm	13.28 ± 0.03	6.04 ± 0.03	1.57	0.68	38.50 ± 0.32
	4.5 µm	14.05 ± 0.04	6.96 ± 0.05	1.36 ± 0.01	0.64	37.28 ± 0.39
PRC B-22 host bulge	g	17.40 ± 0.04	1.22 ± 0.001	1.04	0.84	60.18 ± 0.18
	r	15.60 ± 0.01	1.88 ± 0.001	1.47	0.73	73.02 ± 0.04
	i	15.25 ± 0.01	1.67 ± 0.001	1.39	0.72	71.94 ± 0.02
	3.6 µm	13.75 ± 0.02	1.58 ± 0.01	0.82	0.74	64.39 ± 0.25
	4.5 µm	14.34 ± 0.01	1.64 ± 0.01	0.85	0.75	56.75 ± 0.29
PRC B-22 host disk	g	16.20 ± 0.02	12.92 ± 0.02	1.67	0.35	97.57 ± 0.02
	r	15.57 ± 0.03	12.53 ± 0.01	0.99	0.36	96.12 ± 0.01
	i	15.53 ± 0.03	9.30 ± 0.01	0.69	0.37	93.18 ± 0.01
	3.6 µm	12.48 ± 0.02	8.73 ± 0.04	1.84	0.54	87.55 ± 0.08
	4.5 µm	13.20 ± 0.02	7.72 ± 0.03	1.75 ± 0.01	0.54	86.92 ± 0.09

After re-composing the three individual component magnitudes into a single number representing the total object—for comparison with literature values, which do not decompose the PRGs—we see (1) general agreement in optical filters, (2) moderate agreement between our IRAC 3.6 µm values and the WISE W1 values in the WISE catalog such that our IRAC 3.6 µm values are up to half a magnitude dimmer than the WISE W1 values in the WISE catalog, and (3) that our IRAC 4.5 µm values are up to a magnitude dimmer than the WISE W2 values in the WISE catalog, in cases where photometry exists for these objects. We believe the differences between the WISE photometry and our IRAC photometry may be attributed to the much lower spatial resolution of the WISE image, leading to the potential blending of the PRG with background and foreground objects, and therefore, choose to use our IRAC photometry.

There are trends present in the photometry:

1. The disks of the host galaxies are invariably the brightest components at a given wavelength, and the Sérsic indices are consistent with disk-dominated structures.
2. The polar rings themselves have very low Sérsic indices, which is common among irregular galaxies [22].
3. The rings are typically the largest components (three to four times the size of the disk), but PRC B-22—where the disk is one to two times larger than the ring—shows that this is not necessarily always the case.

4. In all galaxies, the bulges are small in comparison with the other components and are nearly circular. In fact, they are small enough to approach the resolution limits of the observing instruments (particularly in SDSS and IRAC imaging), which may be why the Sérsic indices of those structures tend to be so low: GALFIT cannot perceive the shape of the light profile within such small scales, so it appears to be flat.

To check the Sérsic indices of the bulges, we replicated our methodology—i.e., the decomposition into bulge and disk components in GALFIT—on ten (10) known lenticular and elliptical galaxies from the SDSS *g* band, and found a systematic result represented in each case: when the galaxy is split into two components, GALFIT assigns a flatter light profile with a low Sérsic index to the smaller component. In some cases, previous studies adopted a similar strategy and observed the same phenomenon (e.g., NGC 4111 in [23] and NGC 5308 in [24]). However, literature studies of these targets take data from a wide range of instruments and filters, so direct one-to-one comparisons of Sérsic indices are not possible.

3.2. SED Fitting

Table 8 lists a few of the parameters for each of the target galaxy components, estimated from SED fitting.

Table 8. Estimated Stellar Ages, Masses and Relative SFRs for the different PRG components.

Galaxy	Component	Age (Gyr)	M_{gas} (10^9 $M_\odot$)	M_* (10^9 $M_\odot$)	% SFR
PRC A-4	polar ring	5.51 ± 2.84	2.63 ± 1.39	3.51 ± 1.41	6.05
	host bulge	5.07 ± 2.79	4.20 ± 2.17	5.96 ± 2.25	16.84
	host disk	5.38 ± 2.81	15.9 ± 7.75	21.9 ± 8.07	77.11
PRC A-5	polar ring	5.33 ± 2.97	1.36 ± 0.56	2.01 ± 0.57	28.65
	host bulge	4.88 ± 2.82	0.79 ± 0.36	1.16 ± 0.37	13.65
	host disk	5.14 ± 2.75	3.73 ± 1.76	5.52 ± 1.85	57.70
PRC A-6	polar ring	5.63 ± 2.83	2.45 ± 1.22	3.29 ± 1.25	14.32
	host bulge	5.17 ± 2.76	1.85 ± 0.90	2.60 ± 0.94	17.48
	host disk	4.89 ± 2.73	5.87 ± 2.88	8.45 ± 3.04	68.20
PRC B-12	polar ring	5.41 ± 2.84	8.28 ± 4.44	11.2 ± 4.59	18.08
	host bulge	5.19 ± 2.78	7.16 ± 3.48	9.96 ± 3.63	18.94
	host disk	5.14 ± 2.80	22.1 ± 11.4	31.0 ± 11.8	62.98
PRC B-22	polar ring	6.81 ± 2.94	14.0 ± 5.58	20.8 ± 5.74	31.43
	host bulge	8.46 ± 1.85	128 ± 40.2	135 ± 36.5	0.36
	host disk	6.49 ± 3.01	31.2 ± 12.9	46.8 ± 13.3	68.21

While we expect the main stellar population within the rings to be younger than that within the hosts, these systems could have emerged from neighboring galaxies of roughly contemporaneous origin. Four of the five PRGs in the sample appear to reflect that PRC A-4, A-5, A-6, and B-12 all have similar ages. PRC B-22 is the outlier in this regard, appearing much older in general, and having a bulge significantly older than the other two components in its system.

In most cases the ring is significantly less massive than the host disk, often by an order of magnitude, and the disk of the host tends to be the most massive of the three components (although in PRC B-22, the bulge appears to be far more massive than the disk). While polar rings could theoretically have a great variety of masses relative to their hosts, each specific gas and stellar mass—in addition to ratios—may discriminate between formation scenarios (e.g., merging versus accretion; [9]). While PRC A-5, A-6, and B-12 all exhibit rings with stellar masses around 30% of those in their respective host galaxies, the stellar

masses of the rings around PRC A-4 and PRC B-22 are about 13% and 11% of those in their hosts, respectively.

Furthermore, the rings appear to contain ∼6–30% of the total star formation in our sample galaxies, comparable to or higher than in the host bulges in some cases.

4. Discussion

In this section, we discuss the statistical properties of PRGs. Figures 2–7 show the distributions of the various derived parameters for our sample of PRGs.

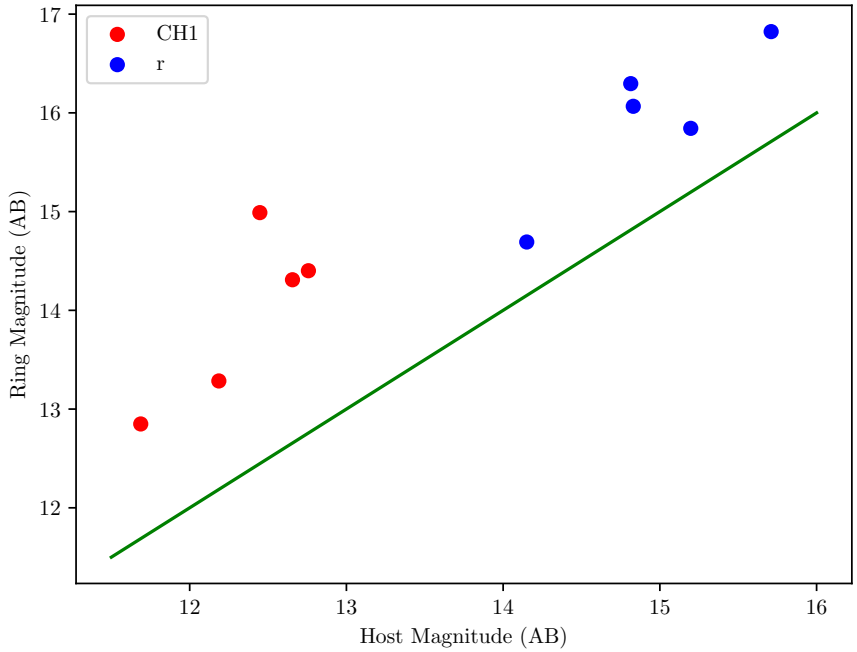

Figure 2. 3.6 μm and r-band magnitudes of the host galaxies of the sample plotted against the same for the polar rings. Green line represents $y = x$, where the magnitudes would be equal, the rings are always dimmer than the host galaxies in this sample.

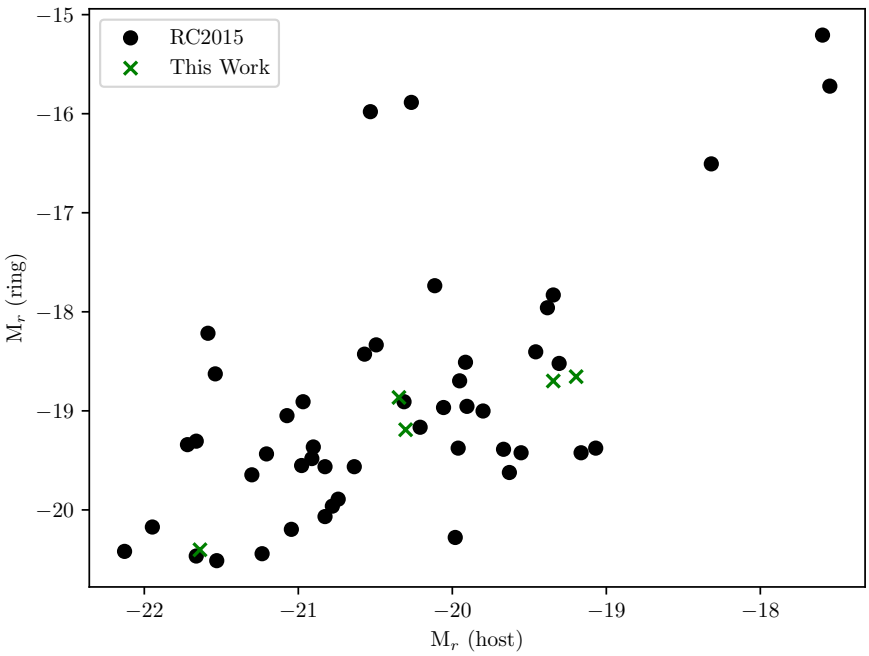

Figure 3. Absolute r-band magnitude for both rings and hosts from this sample overlaid on the same from [3].

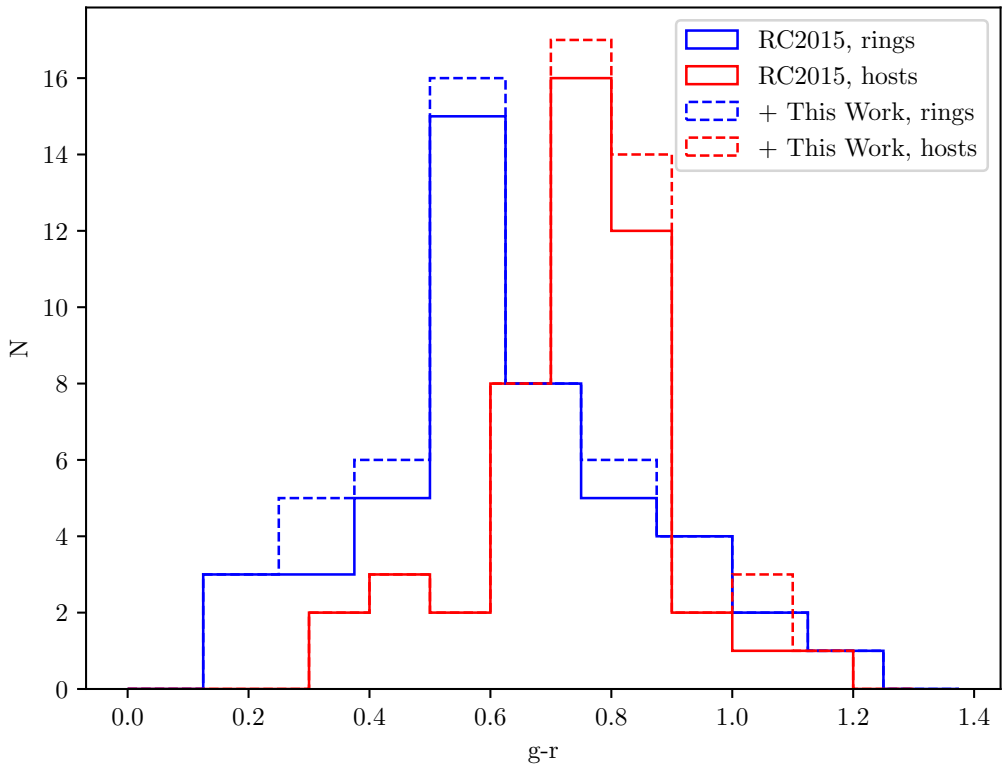

Figure 4. *g-r* color for both rings and hosts from this sample stacked with the same from [3].

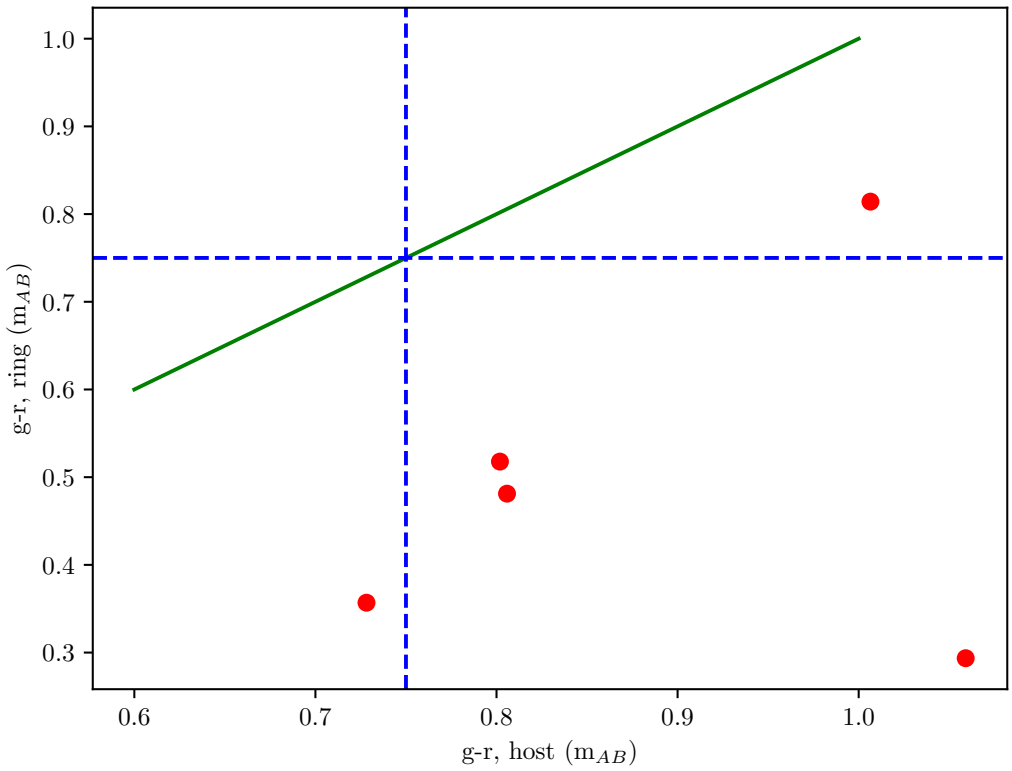

Figure 5. *g-r* of the host versus *g-r* of the ring. Rings in this sample are always bluer than their hosts. Green line represents $y = x$. Dashed blue lines mark $g\text{-}r = 0.75$, below which an object may be considered highly star-forming [25].

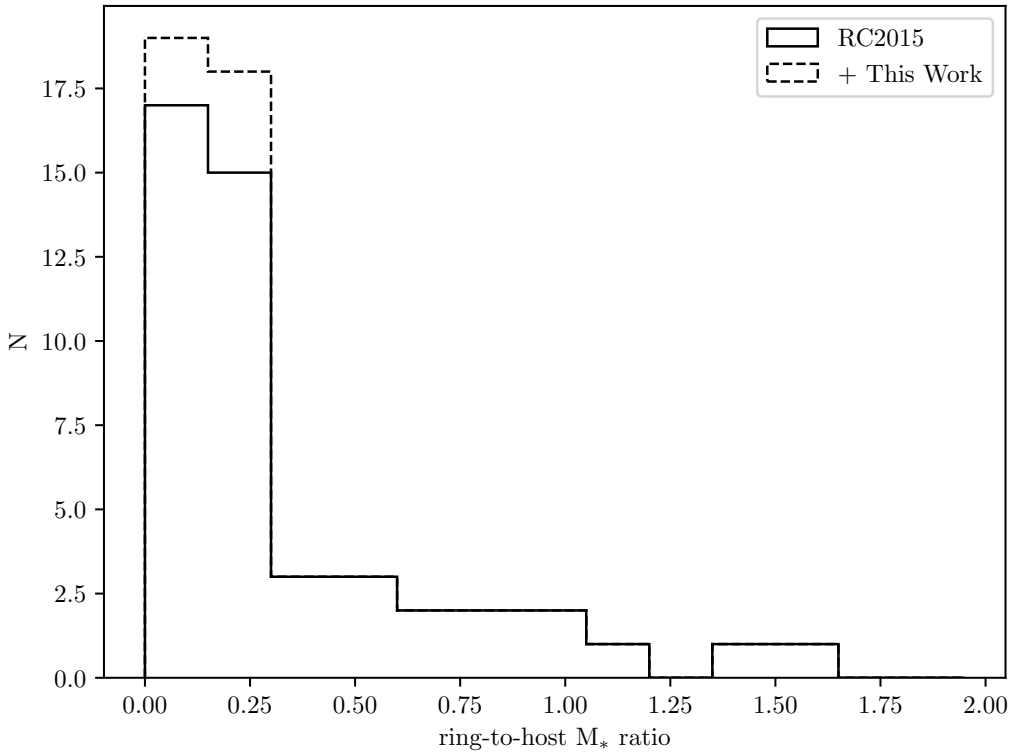

Figure 6. Ring-to-host stellar mass ratio of this sample stacked with the same from [3].

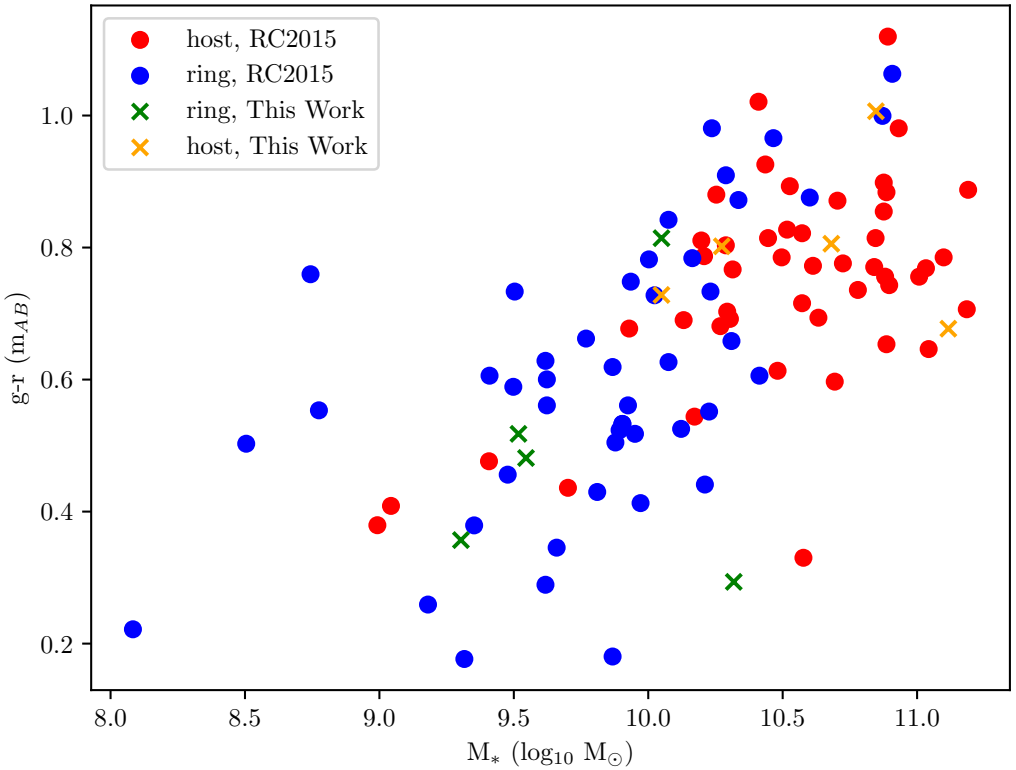

Figure 7. Stellar mass vs. *g-r* color for both rings and hosts from this sample overlaid on the same from [3].

4.1. Geometry

The angle of offset of the ring relative to the polar axis of the host is useful to estimate the ring's origins. With this in mind, the average offsets of the rings of PRC A-4, A-5,

A-6, B-12, and B-22 are 10.2°, 10.7°, 19.4°, 9.3°, and 36.7°, respectively. These values are within expectations set by previous studies (e.g., [3,26]). In particular, the offsets of the rings of PRC A-4, A-5, and B-12 fall within the most frequent measurements for known PRGs. The offset of the ring of PRC B-22 is large with respect to the other four and relatively uncommon within PRGs; furthermore, it lends itself as evidence to the theory that its ring formed as a result of an accretion scenario since a merger is much more likely to develop a ring with a small offset angle. Additionally, such an angle may indicate that the polar structure is much older than the others in the sample, stable rings tend to fall towards the galactic plane as they age on Gyr timescales [27].

Examining the Sérsic indices we see that the rings and bulges within our sample are not concentrated at their centers, their light is spread somewhat evenly throughout their spans and falls off rapidly. This is expected for the rings. This is the advantage of observing rings that are edge-on to observations: they are uniform structures for the most part. The disk profiles tend towards the natural exponential disk profile at $n = 1$, with some variation at infrared wavelengths.

In contrast to the rings, the Sérsic indices of the bulges should not be taken as physically meaningful. We expect a bulge to have a Sérsic index of around 4—the de Vaucouleurs model—shared by early-type galaxies, but that is not the case in this sample. We believe this is because the effective radii of the bulge components are so small that they approach the resolution limits of their respective observing instruments in most cases, at which point GALFIT fails to properly characterize the shapes of their light profiles. Thus, we obtain flat light profiles with no central concentration.

We note that Sérsic indices are not suitable for characterizing galaxies that may be interacting or merging, as irregular and disk-dominated galaxies have plenty of overlap in such schema [28]. With that being said, irregular galaxies do tend to have low values of n, commonly $n < 1.0$ and even $n < 0.5$, so in that regard the profiles of the rings are in agreement with previous studies, if we assume they are irregular structures (e.g., [22]). The exception to this in our sample is the ring of PRC B-12, which itself would appear to be a "disc-dominated" structure with a Sérsic index of $n\sim1.5$ at optical wavelengths.

4.2. Magnitude and Colors

The flux values estimated from our photometry of the individual components may be combined in order to compare to literature values. Doing so, we find that our photometry is in good agreement with previous studies (e.g., [29–32]). The exception to this lies with archival W2 data from WISE, which has a good overlap with IRAC 4.5 μm in terms of wavelength coverage, as mentioned above.

Figure 2 shows the relationship between host (bulge + disk) magnitude and ring magnitude within our sample. It is clear that the ring is always dimmer than the host galaxy, and furthermore, the relationship between the two parameters appears to follow a linear trend. Additionally, when converting these apparent magnitudes to absolute magnitudes ($\mathcal{M}$), they fit in perfectly with trends observed between $\mathcal{M}_{ring}$ and $\mathcal{M}_{host}$ in previous studies (e.g., [3]; see our Figure 3).

The colors of the hosts of PRC A-4, A-5, A-6, B-12, and B-22 fit well within the property parameter space in previous studies (e.g., [3]; see our Figure 4). According to [33], this places the hosts of A-4, A-5, and A-6 into the realm of S0 galaxies. B-12 and B-22 both have redder colors but are comparable to observations for some other PRGs [34]. PRC A-4, PRC A-5, and PRC A-6 are bluer than a normal early-type galaxy (ETG), while B-12 and B-22 fit best as dusty ETGs.

The colors of the rings of PRC A-4, A-5, A-6, B-12, and B-22 also fit well within samples in previous studies (e.g., [3]; see our Figure 4). Referring to [33] once more, the colors of the rings of A-4 and A-6 are akin to normal spiral galaxies, the colors of the rings of A-5 and B-22 are those of an irregular galaxy, and B-12's ring has the color of an S0 galaxy.

Figure 5 shows the relationship between host (bulge + disk) color and ring color, for this work, in *g*-*r*. In all five cases, the rings are bluer than their host galaxies. Also

plotted are lines where g-$r = 0.75$, below which an object is often considered to be highly star-forming [25]. Note, that four of the five polar rings fulfill this condition, and the fifth polar ring nearly does, whereas only one of the five host galaxies fulfills this condition.

4.3. Age

Our results for the ages of the components of some of the PRG systems are surprising. Presumably, the host galaxy and the object it interacted with are both older than the ring. Furthermore, one theory of PRG formation holds that the stars within a polar ring should always be younger than the PRG system itself, a polar ring will not inherit stars from its predecessors [9]. Thus, one would expect the polar ring to be younger than the host galaxy. However, recent simulations indicate that the tidal stripping of a stellar component of a satellite or companion galaxy is possible, meaning that some stars within the ring could be older than the ring itself [27].

We also note that CIGALE gives the age of the main stellar population according to the prescribed star formation history module, not the age of the galaxy within which that stellar population resides. So, any given star within either the ring or the host galaxy could be either younger or older than the polar ring system itself, meaning that the stellar population ages need not have much bearing on the age of the polar ring structure.

On the other hand, in the case of a polar ring forming through a merger, a significant amount of gas from the victim galaxy is expected to fall onto the center of the host galaxy, triggering 2–3 Gyr of "rapid" star formation [9]. This was considered in the SED-fitting through the use of the "sfhdelayed" module for star formation history, in the expectation that the components would undergo some disturbance or surge of activity once the polar ring had formed. In this situation, it is possible that stars within the bulge of the host may be younger than stars within the polar ring. We also note that the uncertainties in the ages are significant due to the small number of photometric bands and Bayesian-like statistics.

Nevertheless, for four of our five PRGs, the estimated ages of the stellar populations within each of the various components are consistent with being similar, although whether that arises from the two progenitor galaxies being contemporaries, or from all of the stellar populations experiencing a new era of star formation after the formation of the ring is not apparent.

The sole outlier is PRC B-22. The stars in the polar ring and host disk appear to be of similar ages, roughly a billion years older than the rest of the sample, and the stars within the bulge are even older. The older age and higher tilt of the ring in PRC B-22 are consistent with the expectations of rings to tilt closer to the galactic plane as they age [27].

4.4. Baryonic Mass

Table 8 shows that the stellar masses of polar rings are significant relative to the stellar masses of their host galaxies, a result that corroborates previous studies (e.g., [3]). The ring-to-host stellar mass ratios of all five galaxies are comparable and similar to those found for other PRGs; see Figure 6. Figure 7 demonstrates the relationship between each component's stellar mass and its color, which is in good agreement with previous studies (e.g., [3]).

We now comment on the implications of our results for PRG formation mechanisms. In the case of a merger, gas from the victim galaxy falls onto the host, where it remains at small radii; under ideal circumstances, as much as 25% of the victim's gas is transferred to the new host, increasing at higher angles of incidence of the collision. In the case of accretion, the rings can maintain masses equal to or even greater than those of the host galaxies [9]. However, our SED-fitting is not capable of tracing the origins of gas, only where stars currently reside.

Regardless, we note that the bulge of PRC B-12 has an estimated gas mass nearly equal to that of its ring, and the bulge of PRC A-4 has an estimated gas mass far higher than that of its ring, though the stellar mass is as well, in the latter case. These notes on A-4 and B-12 may be evidence in favor of mergers, though they are inconclusive, a progenitor

host galaxy could simply be more massive than the eventual ring, even in the event of tidal accretion.

The outlier, at least in terms of absolute numbers, is PRC B-22, which has a disproportionately higher bulge mass, although the measurement of ring-to-host stellar mass ratio for this galaxy (∼11%) is comparable to the ratios commonly seen in other PRGs. However, this is the only case in our sample where the bulge is more massive than the disk. This may be why the ring of PRC B-22 is smaller than the disk (Table 7).

4.5. Implications for Formation Scenarios for Our Five PRGs

As mentioned above, there are three prevailing models for the formation of polar ring galaxies: mergers between two disk galaxies of unequal mass, accretion by tidal stripping of a companion's or satellite's stellar and/or gas component, and cold accretion of pristine gas along cosmic filaments. While both the merging and accretion scenarios are independently able to explain every known polar ring, some differences are expected in physical parameters in the different scenarios; see [9,35,36]. For example:

1. A merger is expected to slightly enrich the center of the host galaxy with infalling gas, without enriching the disk.
2. A merger requires a high mass ratio of two merging galaxies to form a massive and extended polar structure.
3. A ring angled far from the polar axis of its host is heavily suggestive of accretion since a merger will typically always produce a ring oriented close to the polar axis.
4. A merger is expected to generate a stellar halo around the host galaxy.
5. Cold accretion from filaments can produce rings of tremendous mass, even in excess of the host (bulge + disk) mass, because there is no known limit to the accreted mass.

We now discuss our results in the context of the above-mentioned five indicators.

1. PRC A-4 and PRC B-12 both possess bulges with an estimated gas mass comparable to or exceeding that of their polar rings. This may be treated as a weak point in favor of the merger scenario for those two galaxies, though it is not a conclusive factor on its own.
2. On the other hand, we see that the masses of the rings are always significant relative to the masses of their host galaxies, so mergers seem less likely in all cases.
3. PRC B-22 is the only PRG in the sample with a polar ring at a high angle of separation from its host polar axis. Given that a merger will almost never do this, it may be treated as a point in favor of the accretion scenario for that galaxy; the inverse is not true for the remaining four galaxies, since an accretion may just as easily produce a ring near the polar axis of its host. However, in the context of the apparent age of the components in B-22, and self-gravitating rings' expected tendency to fall toward the galactic plane, we may simply be seeing an old ring engaging in normal behavior.
4. Our study does not probe the stellar halos of the host galaxies, so the fourth indicator is beyond the scope of this work.
5. None of the ring masses exceed the host (bulge + disk) masses, so there is no conclusive evidence on this front. However, this also does not mean that none of the rings formed through cold accretion from cosmic filaments either.

The merger scenario is more constrained in terms of the distance between interacting galaxies and their relative velocities, as well as the angles of incidence and gas distribution within the future host. Therefore, although the five PRGs in our study could have formed in galaxy mergers, the accretion scenario may be more likely for these PRGs [9]. The angle of separation between the ring of PRC B-22 and the polar axis of its host is suggestive of tidal accretion. We note that future spectroscopic observations would help to better understand the formation of the sample PRGs, since low gas metallicities (e.g., less than 0.5 $Z_{\odot}$) in the polar ring would be indicative of the accretion of cold gas along cosmic filaments [36].

We note in this context that PRC A-4, B-12, and B-22 are relatively isolated galaxies (with no possible bright companions with an estimated crossing time less than 1 Gyr), PRC

A-6 is somewhat less isolated (with three such possible companion galaxies), and PRC A-5 is in a richer environment (16 possible companion galaxies), based on the study of PRG environments by [37]. Earlier studies (e.g., [37]) found no statistical difference between the environments of PRGs and normal galaxies. However, more recent studies have found that PRG environments are found to be less dense than those of other early-type galaxies [34,38].

4.6. Comparison with Previous Works

We now compare our results with those of past PRG studies. Figures 3, 4, 6 and 7 above show comparisons of our results with those from [3], who used SDSS images to study basic relations between host and ring properties of 50 PRGs. One key difference between our methods and those of [3] is that we have separated the host galaxy into the bulge and disk components, while [3] did not do so. Another key difference is the much larger wavelength coverage of our data, which gives a more comprehensive understanding of each PRG system. Despite these differences, it is still instructive to examine how our results compare to those of [3].

It is clear from Figures 3, 4, 6 and 7 that the absolute magnitudes, the *g*-*r* colors, the ring-to-host stellar mass ratios, and relations between *g*-*r* color index and stellar mass—for both host (bulge + disk) galaxies and polar rings—are in good agreement with the results of [3].

Table 9 compares our results for the ring and host masses in PRC A-4, A-5, and A-6 with those from [36]. Though no uncertainties are available for the literature values, we see reasonable agreement within $\sim 1\sigma$ between our results and the literature values for the ring baryonic masses for A-4 and A-6 and the host baryonic masses for A-5 and A-6. Similarly, our result and the literature values for the host baryonic mass of A-4 differ by about 2σ. On the other hand, we find a substantially different baryonic mass than the literature value for the ring of PRC A-5, especially relative to its corresponding host mass.

The reason for observed discrepancies may be the differing methodologies: degeneracies in SED fitting contribute substantially to the uncertainties in our measurements, and may cause an inappropriate model result to be selected over the "true" result [36], on the other hand, calculated stellar mass from Oxygen abundances using the mass-metallicity relation derived by [39].

Table 9. Comparison of our results with those of [36].

[36]	Host Mass ($10^9 M_\odot$)	Ring Mass ($10^9 M_\odot$)
PRC A-4	7.86	2.88
PRC A-5	5	12
PRC A-6	10.0	3.05
This Work	**Host Mass ($10^9 M_\odot$)**	**Ring Mass ($10^9 M_\odot$)**
PRC A-4	47.96 ± 20.24	6.14 ± 2.8
PRC A-5	11.2 ± 4.34	3.37 ± 1.04
PRC A-6	18.77 ± 7.72	5.74 ± 1.69

We also note that [36] and references therein rule out the merger scenario for both PRC A-4 and PRC A-6 based on kinematics and mass ratios of the two theoretical, interacting systems. Our work corroborates those results, mergers do not appear likely, given that the ring masses are nearly the same order of magnitude as their host masses [36] and references therein go on to conclude that the ring of PRC A-5 formed via the cold accretion scenario, a result we could not corroborate based on high uncertainties in estimations of gas metallicities.

While [36] also cites measurements of ring SFRs based on H_α emission detection, they do not report on other components of the PRGs, making it difficult to directly compare their results to ours.

4.7. Considerations for Future Work

One essential improvement in future works would be to expand the photometry available for these PRGs. SED fitting is particularly dependent on the wavelength range spanned by a data set, and having too few wavebands in a sample can fall prey to degeneracies in models, many galaxies can have similar profiles across specific wavebands, but wildly different physical parameters. This problem can be addressed by sampling photometry at more wavelengths. In the case of these galaxies, sampling more near-infrared bands (e.g., J, H, and K in 2MASS data) or near- and far-ultraviolet bands (e.g., NUV and FUV in GALEX data) can often be enough; however, very often what data exist at these wavelengths shows little to no structure in the PRGs and cannot be decomposed according to our methodology.

What is more, recent studies indicate that as many as half of PRGs host an active galactic nucleus (AGN) of some strength [40]. An expansion of our methodology would be to search for those, whether in photometry or SED fitting. In fact, we attempted this, as seen in the GALFIT residuals in Figure 1, some of the galaxies in our sample may have bright nuclear sources. However, in our case, these structures were at or below the resolution of the instruments. With higher spatial resolution imaging, a fourth component may be added to the photometry in an attempt to model an AGN at the center of each host galaxy. Furthermore, CIGALE is equipped with modules that can model AGNs; those may be incorporated into the SED fitting, even with a three-component setup like ours, but care must be taken to apply AGN modules only to the host bulge component.

Finally, expanding the available population of PRGs is an important task, but not a trivial one. Catalogs of PRGs are limited largely to very nearby galaxies and often require that the ring be edge-on and imaged with sufficient resolution such that a ring is even visible at all. Some recent catalogs of new PRG candidates (e.g., [5]) depend on citizen science efforts such as the Galaxy Zoo Project to collect objects. Such efforts can in principle make it possible to efficiently examine deep images obtained with current/future telescopes, thus speeding up PRG discoveries.

In a similar fashion, machine learning can be employed to automate searches through large surveys such as SDSS or GAIA, and future, equivalent surveys obtained with the upcoming extremely large telescopes. Training a neural network to identify PRGs is possible thanks to existing imaging data, with each "waveband version" of each PRG potentially providing a sample for learning. Given that neural networks often require a very large number of instances for training purposes, the current population of PRGs may seem woefully inadequate, but with upcoming/future deep galaxy surveys similar to those mentioned above, it should be possible to build sufficiently large training sets of PRGs for future machine learning-based PRG searches. Indeed, efforts are already underway to automate the process of finding new PRG candidates using neural networks [41].

5. Conclusions

We have conducted a multi-wavelength photometric study on five PRGs taken from the PRC catalog utilizing optical and infrared imaging with the goal of better-characterizing properties such as stellar mass in these peculiar galaxies. We decomposed objects that have historically been treated as single components and considered infrared data that, in many cases, did not exist at the time of the prior study. In general, our optical photometry was in good agreement with previous results (in cases where previous observations existed), while our infrared photometry likely improved over previous studies due to superior instrumentation. For example, we find that PRC B-12 and PRC B-22 obey the photometric trends observed in PRGs in previous studies. Indeed, the photometric trends for our overall sample are also consistent with trends found in previous studies.

In terms of the SED fitting and baryonic mass, our findings corroborate previous studies while also demonstrating that PRC B-12 and PRC B-22 fall within trends observed in PRGs. Higher-resolution imaging and photometry covering more bands are essential in order to more robustly constrain other physical properties (e.g., SFR, gas metallicity) of

the rings and the hosts. Consequently, such improvements are necessary to constrain the formation scenarios for the polar rings.

While SED fitting is a promising approach, and our estimations of stellar mass generate good agreement with previous studies, the need to use multi-band photometry poses an immediate challenge for many PRGs, which chronically lack good wavelength coverage. Furthermore, PRGs are necessarily self-interacting systems, and treating each component as a separate object may preclude essential characteristics of the system. Nevertheless, with a greater variety of observations of PRGs across the electromagnetic spectrum, this methodology can be improved in the future. Finally, we note that integral field spectroscopy providing information on the kinematics of the stars and gas will be invaluable for understanding the nature, environment, and formation of polar rings.

Author Contributions: Conceptualization, V.P.K. and M.C.A.; methodology, K.E.L., V.P.K. and M.C.A.; software, K.E.L.; validation, V.P.K. and M.C.A.; formal analysis, K.E.L.; investigation, K.E.L.; resources, K.E.L. and V.P.K.; data curation, K.E.L.; writing—original draft preparation, K.E.L.; writing—review and editing, K.E.L., V.P.K. and M.C.A.; visualization, K.E.L.; supervision, V.P.K. and M.C.A.; project administration, V.P.K.; funding acquisition, K.E.L. and V.P.K. All authors have read and agreed to the published version of the manuscript.

Funding: This research was funded from a graduate student research fellowship from South Carolina Space Grant Consortium, from NASA/Spitzer Science Center support for GO programs 70165 and 80194 (PI Kulkarni), and from support received from the University of South Carolina's Office of Research as well as the South Carolina Honors College.

Data Availability Statement: All imaging data in this study are available online from the Spitzer Heritage Archive, SDSS DR6, the Hubble Legacy Archive, and the Gemini Observatory Archive.

Acknowledgments: We thank the anonymous reviewers for constructive comments that have helped to improve our paper.

Conflicts of Interest: The authors declare no conflicts of interest.

References

1. Whitmore, B.C.; Lucas, R.A.; McElroy, D.B.; Steiman-Cameron, T.Y.; Sackett, P.D.; Olling, R.P. New Observations and a Photographic Atlas of Polar-Ring Galaxies. *Astron. J.* **1990**, *100*, 1489–1522. [CrossRef]
2. Deg, N.; Palleske, R.; Spekkens, K.; Wang, J.; Jarrett, T.; English, J.; Lin, X.; Yeung, J.; Mould, J.R.; Catinella, B; et al. WALLABY pilot survey: The potential polar ring galaxies NGC 4632 and NGC 6156. *Mon. Not. R. Astron. Soc.* **2023**, *525*, 4663–5684. [CrossRef]
3. Reshetnikov, V.; Combes, F. Polar-ring galaxies: The SDSS view on the symbiotic galaxies. *Mon. Not. R. Astron. Soc.* **2015**, *447*, 2287–2294. [CrossRef]
4. Reshetnikov, V.P.; Faúndez-Abans, M.; de Oliveira-Abans, M. Polar-ring galaxies: New candidates and statistics. *Astron. Lett.* **2011**, *37*, 171–180. [CrossRef]
5. Moiseev, A.V.; Smirnova, K.I.; Smirnova, A.A.; Reshetnikov, V.P. A new catalogue of polar-ring galaxies selected from the Sloan Digital Sky Survey. *Mon. Not. R. Astron. Soc.* **2011**, *418*, 244–257. [CrossRef]
6. Reshetnikov, V.P.; Mosenkov, A.V. New candidates to polar-ring galaxies from the Sloan Digital Sky Survey. *Mon. Not. R. Astron. Soc.* **2019**, *483*, 1470–1480 [CrossRef]
7. Reshetnikov, V.; Sotnikova, N. Global structure and formation of polar-ring galaxies. *arXiv* **1997**, arXiv:astro-ph/9704047.
8. Bekki, K. Formation of Polar-Ring S0 Galaxies in Dissipative Galaxy Mergers. *Astrophys. J.* **1997**, *490*, L37–L40. [CrossRef]
9. Bournaud, F.; Combes, F. Formation of polar ring galaxies. *Astron. Astrophys.* **2003**, *401*, 817–833. [CrossRef]
10. Macció, A.V.; Moore, B.; Stadel, J. The Origin of Polar Ring Galaxies: Evidence for Galaxy Formation by Cold Accretion. *Astrophys. J.* **2006**, *636*, L25–L28. [CrossRef]
11. Brook, C.B.; Governato, F.; Quinn, T.; Wadsley, J.; Brooks, A.M.; Willman, B.; Stilp, A.; Jonsson, P. The Formation of Polar Disk Galaxies. *Astrophys. J.* **2008**, *689*, 678–686. [CrossRef]
12. Bekki, K. Formation of a Polar Ring Galaxy in a Galaxy Merger. *Astrophys. J.* **1998**, *499*, 635–649. [CrossRef]
13. Makovoz, D.; Khan, I. Mosaicking with MOPEX. In Proceedings of the Astronomical Data Analysis Software and Systems XIV, Pasadena, CA, USA, 24–27 October 2004; pp. 81–85.
14. Labrie, K.; Anderson, K.; Cárdenes, R.; Simpson, C.; Turner, J.E.H. DRAGONS—Data Reduction for Astronomy from Gemini Observatory North and South. In Proceedings of the Astronomical Data Analysis Software and Systems XXVIII, College Park, MD, USA, 11–15 November 2018; pp. 321–324.

15. Peng, C.Y.; Ho, L.C.; Impey, C.D.; Rix, H.-W. Detailed Structural Decomposition of Galaxy Images. *Astron. J.* **2002**, *124*, 266–293. [CrossRef]
16. Peng, C.Y.; Ho, L.C.; Impey, C.D.; Rix, H.-W. Detailed Decomposition of Galaxy Images, II, Beyond Axisymmetric Models. *Astron. J.* **2010**, *139*, 2097–2129. [CrossRef]
17. Bertin, E.; Arnouts, S. SExtractor: Software for source extraction. *Astron. Astrophys. Suppl. Ser.* **1996**, *117*, 393–404. [CrossRef]
18. Boquien, M.; Burgarella, D.; Roehlly, Y.; Buat, V.; Ciesla, L.; Corre, D.; Inoue, A.K.; Salas, H. CIGALE: A python Code Investigating GALaxy Emission. *Astron. Astrophys.* **2019**, *622*, A103. [CrossRef]
19. Bruzual, G.; Charlot, S. Stellar population synthesis at the resolution of 2003. *Mon. Not. R. Astron. Soc.* **2003**, *344*, 1000–1028. [CrossRef]
20. Calzetti, D.; Armus, L.; Bohlin, R.C.; Kinney, A.L.; Koornneef, J.; Storchi-Bergmann, T. The Dust Content and Opacity of Actively Star-forming Galaxies. *Astrophys. J.* **2000**, *533*, 682–695. [CrossRef]
21. Dale, D.A.; Helou, G.; Magdis, G.E.; Armus, L.; Díaz-Santos, T.; Shi, Y.A. Two-parameter Model for the Infrared/Submillimeter/Radio Spectral Energy Distributions of Galaxies and Active Galactic Nuclei. *Astrophys. J.* **2014**, *784*, 83. [CrossRef]
22. Kartaltepe, J.S.; Rose, C.; Vanderhoof, B.N.; McGrath, E.J.; Costantin, L.; Cox, I.G.; Aaron Yung, L.Y.; Kocevski, D.D.; Wuyts, S.; Ferguson, H.C.; et al. CEERS Key Paper, III, The Diversity of Galaxy Structure and Morphology at z = 3–9 with JWST. *Astrophys. J. Lett.* **2023**, *946*, L15. [CrossRef]
23. Richings, A.J.; Uttley, P.; Körding, E. The connection between radio loudness and central surface brightness profiles in optically selected low-luminosity active galaxies. *Mon. Not. R. Astron. Soc.* **2011**, *415*, 2158–2172. [CrossRef]
24. Krajnović, D.; Alatalo, K.; Blitz, L.; Bois, M.; Bournaud, F.; Bureau, M.; Cappellari, M.; Davies, R.L.; Davis, T.A.; de Zeeuw, P.T.; et al. The ATLAS^{3D} project—XVII. Linking photometric and kinematic signatures of stellar discs in early-type galaxies. *Mon. Not. R. Astron. Soc.* **2012**, *432*, 1768–1795. [CrossRef]
25. Kouroumpatzakis, K.; Zezas, A.; Kyritsis, E.; Salim, S.; Svoboda, J. Star formation rate and stellar mass calibrations based on infrared photometry and their dependence on stellar population age and extinction. *Astron. Astrophys.* **2023**, *673*, A16. [CrossRef]
26. Smirnova, K.I.; Moiseev, A.V. Are Polar rings indeed polar? *Astrophys. Bull.* **2013**, *68*, 371–380. [CrossRef]
27. Smirnov, D.V.; Mosenkov, A.V.; Reshetnikov, V.P. Polar-ring galaxies in the Illustris TNG50 simulation. *Mon. Not. R. Astron. Soc.* **2024**, *527*, 4112–4128. [CrossRef]
28. LaChance, P.; Croft, R.; Ni, Y.; Chen, N.; Di Matteo, T.; Bird, S. The evolution of galaxy morphology from redshift z = 6 to 3: Mock JWST observations of galaxies in the ASTRID simulation. *arXiv* **2024**, arXiv:2401.16608.
29. Explanatory Supplement to the AllWISE Data Release Products. Available online: https://wise2.ipac.caltech.edu/docs/release/allwise/expsup/index.html (accessed on 4 April 2024).
30. Lauberts, A.; Valentijn, E.A. *The Surface Photometry Catalogue of the ESO-Uppsala Galaxies*; European Southern Observatory: Munich, Germany, 1989.
31. de Vaucouleurs, G.; de Vaucouleurs, A.; Corwin, H.G., Jr.; Buta, R.J.; Paturel, G.; Fouque, P. *Third Reference Catalogue of Bright Galaxies*; Springer: New York, NY, USA, 1991.
32. Adelman-McCarthy, J.K.; Agüeros, M.A.; Allam, S.S.; Allende Prieto, C.; Anderson, K.S.J.; Anderson, S.F.; Annis, J.; Bahcall, N.A.; Bailer-Jones, C.A.L.; Baldry, I.K.; et al. The Sixth Data Release of the Sloan Digital Sky Survey. *ApJ Suppl. Ser.* **2008**, *175*, 297–313. [CrossRef]
33. Fukugita, M.; Nakamura, O.; Okamura, S.; Yasuda, N.; Barentine, J.C.; Brinkmann, J.; Gunn, J.E.; Harvanek, M.; Ichikawa, T.; Lupton, R.H.; et al. A Catalog of Morphologically Classified Galaxies from the Sloan Digital Sky Survey: North Equatorial Region. *Astron. J.* **2007**, *134*, 579–593. [CrossRef]
34. Finkelman, I.; Funes, J.G.; Brosch, N. Polar Ring galaxies in the Galaxy Zoo. *Mon. Not. R. Astron. Soc.* **2012**, *422*, 2386–2398. [CrossRef]
35. Bournaud, F.; Jog, C.J.; Combes, F. Galaxy mergers with various mass ratios: Properties of remnants. *Astron. Astrophys.* **2005**, *437*, 69–85. [CrossRef]
36. Spavone, M.; Iodice, E.; Arnaboldi, M.; Longo, G.; Gerhard, O. Chemical abundances of the PRGs UGC 7576 and UGC 9796. I. Testing the formation scenario. *Astron. Astrophys.* **2011**, *531*, A21. [CrossRef]
37. Brocca, C.; Bettoni, D.; Galletta, G. The visible environments of polar ring galaxies. *arXiv* **1997**, arXiv:astro-ph/9706153.
38. Savchenko, S.S.; Reshetnikov, V.P. Spatial environment of polar-ring galaxies from the SDSS. *Astron. Lett.* **2017**, *43*, 146–151. [CrossRef]
39. Tremonti, C.A.; Heckman, T.M.; Kauffmann, G.; Brinchmann, J.; Charlot, S.; White, S.D.M.; Seibert, M.; Peng, E.W.; Schlegel, D.J.; Uomoto, A.; et al. The origin of the mass-metallicity relation: Insights from 53,000 star-forming galaxies in the Sloan digital sky survey. *Astrophys. J.* **2004**, *613*, 898–913. [CrossRef]
40. Smirnov, D.V.; Reshetnikov, V.P. Active Galactic Nuclei among Polar-Ring Galaxies. *Astron. Lett.* **2020**, *46*, 501–508. [CrossRef]
41. Kirmani, F.; Lackey, K.E.; Kulkarni, V.P.; Rodney, S.; Rose, J.R. Detecting Polar Ring Galaxies via Deep Learning. *RASTI* 2024, *submitted*.